14th International Symposium on Turbulence and Shear Flow Phenomena (TSFP14)
Heidelberg, Germany, July 28-31, 2026

UNCERTAINTY IN STATE ESTIMATION OF TURBULENT CHANNEL FLOW FROM WALL OBSERVATIONS

Fan Fei
Department of Mechanical Engineering
The University of Tokyo
7-3-1 Hongo, Bunkyo-Ku, Tokyo 113-8656, Japan
feifan@iis.u-tokyo.ac.jp

Ming Liu
Center for Research on Innovative Simulation Software
Institute of Industrial Science
The University of Tokyo
4-6-1 Komaba, Meguro-ku, Tokyo 153-8505, Japan
liuming@iis.u-tokyo.ac.jp

Yosuke Hasegawa
Center for Research on Innovative Simulation Software
Institute of Industrial Science
The University of Tokyo
4-6-1 Komaba, Meguro-ku, Tokyo 153-8505, Japan
ysk@iis.u-tokyo.ac.jp

ABSTRACT

Estimation of turbulent flows from limited measurements is a long-standing challenge, particularly for a channel flow where wall information weakly correlates with the outer-layer dynamics. In the present study, an adjoint-variational approach is employed to estimate a flow state of a fully developed turbulent channel flow with wall measurements. Multiple estimates are generated by assimilating the same wall measurement from different initial conditions, and their ensemble mean and standard deviation are subsequently analysed. The standard deviation among the different estimates is smaller than the fluctuations of the ensemble mean within the near-wall region of 50 in the wall unit, while their deviation become prominent outside the region, suggesting the non-uniqueness of a flow state in the outer layer. Furthermore, the region with a high standard deviation value is observed to shift from the high-speed streaks to the low-speed streaks as it moves away from the wall, indicating that the predictions of sweep in the inner layer and ejection in the buffer layer are particularly challenging and have larger uncertainty.

INTRODUCTION

Estimation of turbulent flows based on limited and possibly noisy measurements is important in flow control and environmental prediction, remaining one of fundamental problems in fluid mechanics. As a representative of non-intrusive observables, wall measurement has often been considered, while the estimation of the complete flow state from the wall information is challenging due to the weak correlation between near-wall and outer-layer dynamics.

Flow estimation strategies for data assimilation are generally categorized into model-based and data-driven approaches. Model-based methods such as adjoint-variational techniques (Bewley and Protas, 2004) and Kalman filtering (Kim and Bewley, 2007) allow to ensure physical consistency of the estimated flow by exploiting the governing equations, while they usually suffer from high computational costs. Data-driven approaches such as linear stochastic estimation (Suzuki and Hasegawa, 2017) and deep neural networks (Cuéllar et al., 2024) are less expensive, while there is no guarantee that their predictions satisfy the governing equations. Regardless of employed schemes, existing studies have commonly shown that only the vicinity region of the wall can be accurately estimated, while the estimation error becomes significant beyond a certain height from the wall. This is primarily caused by the inherent ill-posedness of a flow estimation problem, where wall information is insufficient to uniquely determined the entire flow state. In the present study, we tackle this problem by an ensemble approach, by conducting multiple estimations based on the same wall measurement, and the statistical properties of the ensembles are analyzed to discuss the variations of possible flow states for the same wall measurements. This allows us to quantify the uncertainty in the flow estimation based on wall measurement.

METHODOLOGY

In this study, direct numerical simulation (DNS) of turbulent channel flow is performed at a bulk Reynolds number of $Re_b = \frac{2U_b h}{\nu} = 5693$ under a constant flow rate, where U_b is the bulk mean velocity, h is the half channel height, and ν is the kinematic viscosity of the fluid. The fluid is assumed to be incompressible and Newtonian, governed by the continuity and Navier–Stokes equations. No-slip boundary conditions are imposed at the top and bottom walls, while periodic boundary conditions are applied in the streamwise (x) and spanwise (z) directions, while the wall-normal direction is denoted by y. DNSs are conducted using the open-source solver Incompact3D (Laizet and Lamballais, 2009). Detailed numerical configurations are summarized in Table 1.

In the present study, the true flow state is obtained from DNS from a particular initial state of a fully developed turbulent channel flow. Then, the space and time evaluation of the wall measurement is extracted. The wall measurement is used for flow estimation starting from a completely uncorrected instantaneous flow field from the fully developed turbulent channel flow under the same Reynolds number as that of the true field. The unique feature of the present study is that we obtain multiple estimations starting from uncorrelated initial fields with the same wall measurement and examine how the multiple estimated flow states evolve in time. As for data assimilation, we employed an adjoint-based method, where the initial flow field following cost function is minimized:

$$J = \frac{1}{2}\int_0^{T^+}\int_S [\alpha_u \frac{1}{Re_b^2}\left(\frac{\partial u}{\partial y} - \frac{\partial u^m}{\partial y}\right)^2_{wall} + \alpha_w \frac{1}{Re_b^2}\left(\frac{\partial w}{\partial y} - \frac{\partial w^m}{\partial y}\right)^2_{wall} + (p-p^m)^2_{wall}] dSdt, \quad (1)$$

where $\alpha_u, \alpha_w, \alpha_p$ are weighing factors; u, w, p are streamwise velocity, spanwise velocity and pressure, respectively, while u^m, w^m, p^m are the corresponding measurements on the wall , and the subscript $wall$ represents the wall quantities. The integration is carried out over the top and bottom walls S, and the assimilation horizon T^+ is set as 50, where the superscript '+' denotes normalization in wall units. This corresponds to one Lyapunov time scale $\tau_\sigma^+ = 50$ (Wang et al., 2022) for channel flow under the same Reynolds number. The adjoint governing equations for minimizing the cost functional (1) can be derived as:

$$\frac{\partial u_i^*}{\partial x_i} = 0, \quad (2)$$

$$\frac{\partial u_i^*}{\partial t^*} - u_j\frac{\partial u_i^*}{\partial x_j} - u_j\frac{\partial u_j^*}{\partial x_i} + \frac{\partial p^*}{\partial x_i} - \frac{1}{Re}\frac{\partial^2 u_i^*}{\partial x_j \partial x_j} = 0, \quad (3)$$

with the following boundary conditions on the two walls:

$$u^*|_{wall} = -\alpha_u \frac{1}{Re}\left(\frac{\partial u}{\partial y} - \frac{\partial u^m}{\partial y}\right), v^*|_{wall} = n_{wall}\alpha_p(p-p^m), \quad w^*|_{wall} = -\alpha_w \frac{1}{Re}\left(\frac{\partial w}{\partial y} - \frac{\partial w^m}{\partial y}\right). \quad (4)$$

Here, the quantity with a superscript * denotes the corresponding adjoint quantity. $n_{wall} = 1$ for the upper wall, whereas $n_{wall} = -1$ for the lower wall.

The adjoint fields are solved backward in time to compute the gradient of the cost functional (1) with respect to a prescribed initial condition $\boldsymbol{u}(\boldsymbol{x}, t = 0)$. The gradient is used to iteratively update the initial condition, and the optimized state after about 200 iterations will serve as the starting point for the next assimilation horizon. Repeating this procedure yields flow estimations up to $t^+ = 1200$ from multiple initial conditions. Totally N = 100 estimates are performed simultaneously by using the wall measurement from the true state.

RESULTS AND DISCUSSIONS

To quantify the uncertainty in the estimates, the ensemble-averaged field and the standard deviation (Std) of the estimates around their ensemble mean are introduced. Also, the root-mean-square of the ensemble-averaged field on the wall-parallel plane of interest is defined to evaluate the fluctuating intensity. Then, their ratio R_ϕ is further calculated to quantify their magnitude as

$$R_\phi(y,t) = \frac{\sigma_{\phi,rms}(y,t)}{\phi_{\text{rms}}(y,t)} = \frac{\sqrt{\left\langle \frac{\sum_{i=1}^N(\phi_{ei} - \tilde{\phi}_e)^2}{N}\right\rangle_{xz}}}{\sqrt{\left\langle\left(\tilde{\phi}_e - \langle\tilde{\phi}_e\rangle_{xz}\right)^2\right\rangle_{xz}}}, \quad (5)$$

where the tilde denotes an ensemble mean as $\tilde{\phi}_e = \frac{\sum_{i=1}^N \phi_{ei}}{N}$, ϕ refers to a flow quantity, i.e., u, v, w, p. $\langle\cdot\rangle_{xz}$ represents a spatial average in the *x*-*z* plane.

Besides, the correlation coefficient C_ϕ between the ensemble-averaged field and the true field is calculated by

$$C_\phi = \frac{\langle\tilde{\phi}_e'\phi_t'\rangle_{xz}}{\langle\tilde{\phi}_e'^2\rangle_{xz}^{\frac{1}{2}}\langle\phi_t'^2\rangle_{xz}^{\frac{1}{2}}}, \quad (6)$$

where the subscript t and e denote estimated and true flow quantities, respectively. A dashed quantity indicates the fluctuation of the quantity by subtracting their corresponding time-averaged values.

Figure 1 shows the temporal evolution of R_ϕ along the wall-normal direction. In the wall-normal direction, R_ϕ increases towards the channel center, as it relies solely on wall measurements. As assimilation proceeds, the decrease of R_ϕ indicates the dependence of the estimation results on the initial values gradually diminishes. Previous study by Wang et al. (2022) shows that, the accurate estimation can only be achieved within $y^+ < 20$. This is further confirmed by multiple estimates in the present study. Due to the limitation of the wall observation, $R_\phi < 1$ is achieved in the vicinity of the wall within $y^+ < 50$, while the uncertainty near the channel center remains large.

Figure 2 shows the temporal evolution of C_ϕ along the wall-normal direction. Initially, high correlation appears only near the wall, while the outer region is essentially uncorrelated. As assimilation proceeds, C_ϕ gradually increases across the wall-normal direction, indicating that the ensemble-averaged field approaches the true field until $t^+ = 1200$.

The similarity between the turbulent structures of the true field and of the ensemble-averaged field is further quantitatively evaluated through the intersection over union of Q criterion IoU_Q, which is defined as the ratio of the region of their intersection to the region of their union by

$$IoU_Q = \frac{|V_e \cap V_t|}{|V_e \cup V_t|}, \quad (7)$$

where V represent the total volume where the local Q criterion is larger than a threshold. A higher IoU_Q, indicates a higher similarity in the vortex structures between estimated and the true fields. Figure 3 presents the temporal evolution of IoU_Q, along the wall-normal direction with a threshold of Q = 0.5. IoU_Q exhibits low values in the outer region $y^+ > 50$, since the ensemble mean filters out fluctuations. In contrast, high values of IoU_Q , appear in the near-wall region $y^+ < 25$. This indicates that wall measurements can reconstruct near-wall turbulent structures with higher fidelity, consistent with the results in Figure 2.

Figure 4 (a) presents the instantaneous streamwise velocity u on the middle plane in the spanwise direction from true and ensemble-averaged field. The ensemble mean smooths out most structures around the channel center, while streaky structures near the wall are reproduced. This indicates that uncertainties due to initial conditions are amplified in the regions dominated by large-scale turbulent structures, highlighting the inherent difficulty of flow estimation due to the chaotic nature of turbulence. To further quantify the similarity among the estimates, Figures 4 (b) and (c) plot instantaneous streamwise velocity u and the Std $\sigma_{\phi,rms}$ among the estimates on the wall-parallel planes $y^+ = 5$ and 50, respectively. The high $\sigma_{\phi,rms}$ region that suggests larger uncertainties are typically collocated with high-speed streaks at $y^+ = 5$, whereas it preferentially appears within low-speed streaks at $y^+ = 50$.

The shift of high $\sigma_{\phi,rms}$ region from high-speed streaks to low-speed streaks as y^+ increases is further illustrated in Figure 5. It plots the probability density functions of $\sigma_{\phi,rms}$ conditioned on different velocity fluctuations u'. As y^+ increases, high $\sigma_{\phi,rms}$ region gradually shifts from high velocity to low velocity. The high-velocity and low-velocity structures are shown by the contour of $u' = 0.1$ and -0.1, respectively, in Figure 6. The high-speed streaks, i.e., $u' = 0.1$, are almost located in the region below $y^+ = 25$ and exhibit negative wall-normal velocity v, indicating a sweeping event in the inner layer. By comparison, the low-speed streaks, i.e., $u' = -0.1$, appear at wall normal location higher than $y^+ = 25$ with positive wall-normal velocity v, suggesting an ejection event in the buffer layer. These dominant dynamical events render the data assimilation more challenging and contribute to the increased estimation uncertainty.

CONCLUSION

In this study, the adjoint-variational method is employed to estimate turbulent channel flows using wall measurements from various initial values. Multiple estimates assimilating the same wall measurements are conducted starting from independent initial fields of a fully developed turbulent channel flow. The results suggest a significant deviation among multiple estimates especially near the channel center. Although the uncertainty gradually decreases as assimilation proceeds, the region with small variation among the multiple estimates is limited to the buffer layer. Moreover, it was also found that the large uncertainty occurs in the sweeping events in the inner layer and the ejection events in the buffer layer. The present study confirms the limitations of state estimation from wall observation, and also allows quantitative evaluation of the uncertainty in the estimation based on limited measurements.

REFERENCES

Bewley, T. R., and Protas, B., 2004, "Skin Friction and Pressure: The ‘Footprints’ of Turbulence," *Physica D*, Vol. 196, pp. 28–44.

Cuéllar, A., Güemes, A., Ianiro, A., Flores, Ó., Vinuesa, R., and Discetti, S., 2024, "Three-Dimensional Generative Adversarial Networks for Turbulent Flow Estimation from Wall Measurements," *J. Fluid Mech.*, Vol. 991, A1.

Kim, J., and Bewley, T. R., 2007, "A Linear Systems Approach to Flow Control," *Annu. Rev. Fluid Mech.*, Vol. 39, No. 1, pp. 383–417.

Laizet, S., and Lamballais, E., 2009, "High-Order Compact Schemes for Incompressible Flows: A Simple and Efficient Method with Quasi-Spectral Accuracy," *J. Comput. Phys.*, Vol. 228, No. 16, pp. 5989–6015.

Suzuki, T., and Hasegawa, Y., 2017, "Estimation of Turbulent Channel Flow at Reτ = 100 Based on the Wall Measurement Using a Simple Sequential Approach," *J. Fluid Mech.*, Vol. 830, pp. 760–796.

Wang, Q., Wang, M., and Zaki, T. A., 2022, "What Is Observable from Wall Data in Turbulent Channel Flow?" *J. Fluid Mech.*, Vol. 941, A48.

Table 1. Domain sizes and grid resolutions normalized by the viscous length scale

L_x/h	L_y/h	L_z/h	N_x	N_y	N_z	Δx^+	Δy^+	Δz^+	Δt^+
6.4	2	3.2	128	129	129	9	0.93~7.9	4.5	0.046

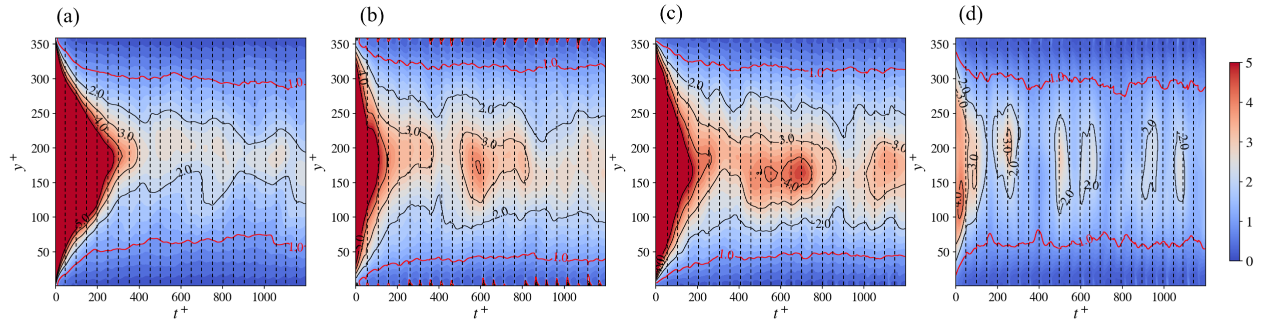

Figure 1. Temporal evolution of ratio of the fluctuation of the ensemble-averaged field and the standard deviation of different estimates for (a) $\boldsymbol{R_u}$, (b) $\boldsymbol{R_v}$, (c) $\boldsymbol{R_w}$, and (d) $\boldsymbol{R_p}$. Hereinafter, the vertical dash dotted lines indicate the time horizon.

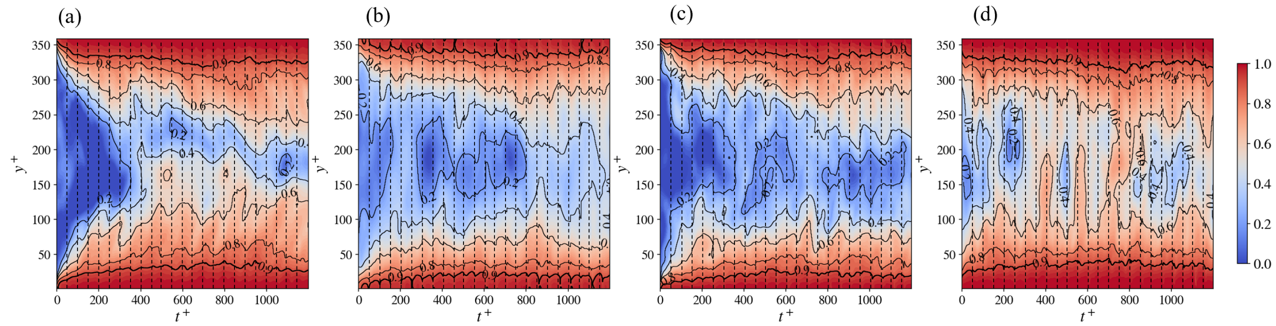

Figure 2. Temporal evolution of correlation coefficient between the ensemble-averaged field and the true field for (a) $\boldsymbol{C_u}$, (b) $\boldsymbol{C_v}$, (c) $\boldsymbol{C_w}$ and (d) $\boldsymbol{C_p}$.

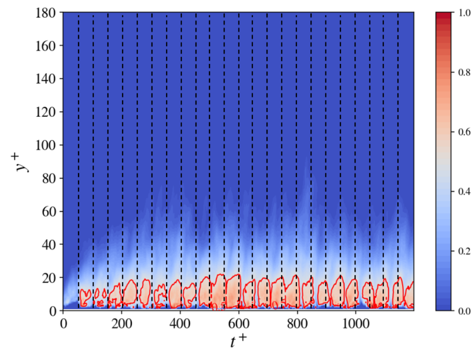

Figure 3. Temporal evolution of $\boldsymbol{IoU_Q}$ along the wall-normal direction of the half channel height with thresholds of $\boldsymbol{Q = 0.5}$. The red solid lines indicate the isoline for $\boldsymbol{IoU_Q = 0.5}$.

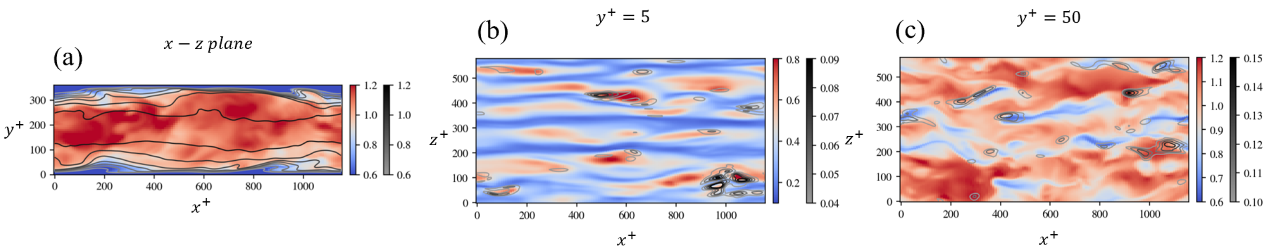

Figure 4. The instantaneous streamwise velocity on (a) the middle plane in the spanwise direction, and the wall-parallel planes (b) $\boldsymbol{y^+ = 5}$ and (c) $\boldsymbol{y^+ = 50}$. All the contours show the true fields, while the isolines show the ensemble-averaged field and the Std field $\boldsymbol{\sigma_{u,rms}}$ of the estimates in Fig. 3(a) and Figs.3 (b)(c), respectively.

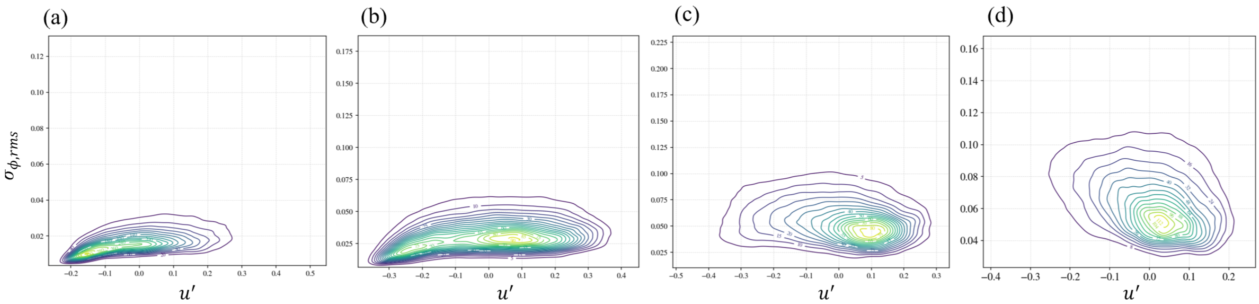

Figure 5. The probability density functions of $\boldsymbol{\sigma_{\phi,rms}}$ conditioned on velocity fluctuations on wall-parallel planes of (a) $\boldsymbol{y^+ = 5}$, (b) $\boldsymbol{y^+ = 10}$, (c) $\boldsymbol{y^+ = 25}$, and (d) $\boldsymbol{y^+ = 50}$.

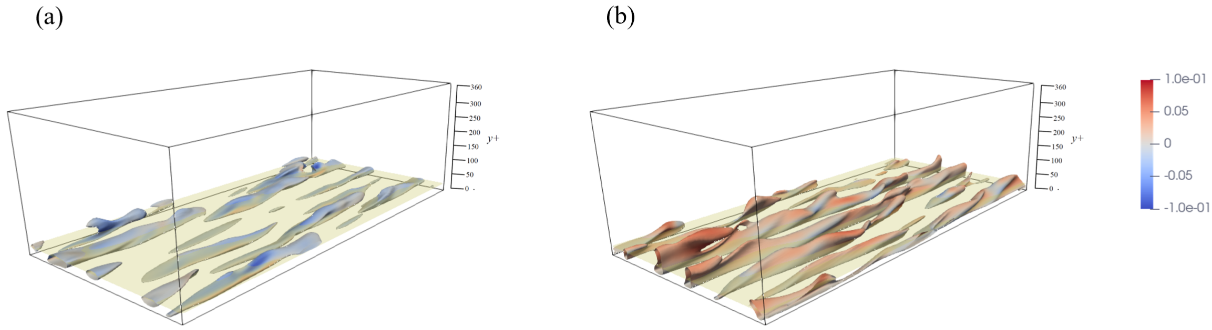

Figure 6. Instantaneous velocity structures shown by the contour of the fluctuating streamwise velocity (a) $\boldsymbol{u' = 0.1}$ and (b) $\boldsymbol{u' = -0.1}$. The surfaces are colored by the wall-normal velocity and the yellow plane indicates $\boldsymbol{y^+ = 25}$